RSC Advances

ROYAL SOCIETY OF CHEMISTRY

www.rsc.org/advances

RSC Advances

RSCPublishing

ARTICLE

Au-Cu-Pt ternary catalyst fabricated by electrodeposition and galvanic replacement with superior methanol electrooxidation activity

Cite this: DOI: 10.1039/xoxxoooooox

Received ooth January 2012,
Accepted ooth January 2012

DOI: 10.1039/xoxxoooooox

www.rsc.org/

Caiqin Wang, Fangfang Ren, Chunyang Zhai, Ke Zhang, Beibei Yang, Duan Bin, Huiwen Wang, Ping Yang, Yukou Du*

A series of Au-Cu-Pt ternary catalysts were fabricated on glassy carbon electrode (GCE) by a two-step method. Au-Cu nanoparticles were formed by initial electrodeposition of Au-Cu layers onto GCE and then followed by the partial replacement of Cu by Pt. The morphology and composition of Au-Cu-Pt catalysts were characterized by scanning electron microscope (SEM), energy dispersive X-ray analysis (EDX), EDX element mapping and X-ray photoelectron spectroscopy (XPS). It was found that the alloying micro-structures existed in the catalysts among Au, Cu and/or the partially replaced Pt. Moreover, electrochemical measurements revealed that although with rather low loading of Pt, Au-Cu-Pt/GCE-10 catalyst presented superior electrocatalytic activity and stability to that of the other comparative electrodes toward methanol electrooxidation (MEO). It indicated that this two-step method can efficiently decrease the amount of Pt loading in catalyst. These findings also suggested that the prepared Au-Cu-Pt catalyst has a great potential for use in direct methanol fuel cell (DMFC).

Introduction

Over decades, a lot of progress has been made in the development of direct methanol fuel cell (DMFC). Nevertheless, its performance still cannot meet the demand of the wide commercialization.[1-3] At present, platinum is generally considered as an excellent anodic catalyst for DMFC because it gives significant activity for methanol electrooxidation (MEO) at low temperatures. But it is restricted in commercial applications due to its high cost, limited supply and readily poisoned by the reaction intermediates generated in the process.[4-6] As a result, the development and characterization of a cheaper and better poison-tolerance catalyst are of tremendous interest to this technology.

Bimetallic nanoparticles are receiving much attention because of their specific electronic, optical and catalytic properties.[7,8] Platinum can be alloyed with other metals to obtain bimetallic materials to overcome the blocking effect of CO-like species. Pt-based bimetallic nanoparticles have also been the choice of catalyst in many important electrochemical reactions, including reduction of oxygen[9] and direct oxidation of methanol.[10] Many investigations indicate the alloying of Pt with other metals significantly enhances the catalytic activity and poisoning tolerance of Pt on the basis of bifunctional mechanism and/or electronic effect.[2,11] Among the various Pt-based bimetallic nanoparticles, PtAu bimetallic nanoparticles are very important because they exhibit excellent catalytic activity and resistance to deactivation due to the highly synergistic interaction between platinum and gold. Au was found to possess catalytic activity for the oxidation of organic compounds.[12] The materials with incorporation of Au into Pt exhibit excellent catalytic activity, enhanced carbon monoxide (CO) tolerance and better stability than Pd/C or Pt/C catalysts.[13] Theoretical study of methanol oxidation on the PtAu(111) bimetallic surface identify that CO possesses larger adsorption energy on the PtAu(111) surface than that on the pure Pt(111) surface, leading to the poor adsorbed CO on PtAu(111) surface. And the non-CO pathway on the bimetallic surface is found to be energetically more favorable than the CO pathway. These calculated results propose that the improved electrocatalytic activity of PtAu bimetallic catalysts for methanol oxidation should be attributed to the alternation in the major reaction pathway from the CO pathway on the pure Pt surface to the non-CO pathway on the PtAu bimetallic surface, rather than the easier removal of CO on PtAu catalysts than that on pure Pt catalysts.[14] According to Xing's work,[15] the CO formation can be reduced gradually with increasing surface Au fractions in PtAu alloys and CO poisoning can be almost eliminated by adjusting to a proper surface Au fraction. In addition, Au-Pt core-shell nanoparticles (Au-Pt NPs) as an effective bimetallic electrocatalyst for methanol oxidation have also been extensively explored.[16] Also, surface composition tuning of Au-Pt bimetallic nanoparticles is crucial for enhanced carbon monoxide and methanol electro-oxidation.[17]

In order to overcome the high cost of platinum catalyst, copper is introduced into the catalyst to reduce the amount of

platinum loading. The addition of Cu to Pt could increase the catalytic activities of methanol oxidation and formic acid oxidation as well.[18] In Ammam's work, binary catalysts containing Pt and Cu have been synthesized by two different methods, it is found that both catalysts show superior catalytic activity towards ethanol electrooxidation compared to pure Pt/C.[19] Wang et al. [20] reported a novel one-pot co-reduction solvothermal approach to obtain concave and dendritic $PtCu_x$ (x = 1, 2 and 3) bimetallic nanoparticles, the mass activity and specific activity of $PtCu_2$/C were 3.3 and 4.1 times higher than those of the commercial Pt/C catalysts, respectively.

In recent decades, Pt-based ternary catalyst has been paid much attention due to its superior catalytic activity and property. In contrast to mono and bi-metallic catalysts, trimetallic Pt-based catalysts exhibit enhanced catalytic activity because they offer much more opportunities for tailoring their properties.[10] And the ternary catalyst can be easily prepared by the simple co-electrodeposition method.[10] Zhang et al.[21] fabricated PtPdAu ternary alloy nanoparticles on graphene with superior methanol electrooxidation activity. In Tsiouvaras' work,[22] ternary (PtRuMo/C) catalysts were fabricated and subjected to thermal reduction at 300 °C in H_2 and He atmosphere, which were more active towards CO and methanol oxidation than binary catalysts. A novel ternary PdCuPb/C nanocatalyst has been fabricated via reducing Cu^{2+} and Pb^{2+} ions on carbon surface followed by Pd^{2+} ion substitution, and it exhibits excellent activity for ethanol electrooxidation in alkaline medium.[23] Ammam et al.[24,25] have recently reported the synthesis, characterization and the catalytic activity of binary PtMn/C and ternary PtMnX/C (X = Fe, Co, Ni, Cu, Mo and Sn) alloys catalysts and found that compared to Pt/C and PtMn/C, overall the ternary alloys catalysts exhibited higher catalytic activities towards ethanol oxidation. Recently, the dendritic Au/Pt and Au/PtCu nanowires were fabricated through an effective, heterogeneous and epitaxial growth strategy and the synthesized products exhibit excellent electrocatalytic activity towards methanol electrooxidation.[26]

The aim of this work has been to fabricate a series of Au-Cu-Pt ternary catalysts on glassy carbon electrode (GCE) and correlate their composition with their electrocatalytic activity toward MEO. In this direction, specific ideas and objectives of this research are as follows: (i) The Au-Cu-Pt ternary catalysts have been fabricated by a simple two-step method. Au-Cu nanoparticles were firstly formed onto GCE by initial electrodeposition, then Cu in Au-Cu nanoparticles was partially replaced by Pt. And the amount of platinum loading is anticipated to be reduced by using this method. (ii) The characterization of the Au-Cu-Pt ternary catalyst and its evaluation of catalytic performances had been performed. It had been found that the alloying micro-structures exist in the catalyst among Au, Cu and/or the partially replaced Pt during the fabrication process. And the optimal scheme for the high activity of catalyst had been found toward the methanol electrooxidation (MEO). (iii) The electronic effect and synergetic effect among the three metals are expected to have a significant positive impact on the catalytic performances.

Experimental

Materials and apparatus

$HAuCl_4$, H_2PtCl_6 (Shanghai shiyi Chemicals reagent Co., Ltd., China), CH_3OH, H_2SO_4 and $CuSO_4$ (Sinopharm Chemicals Reagent Co., Ltd., China) were all of analytical grade and used without further purification. Doubly distilled water was used throughout the experiments. The solutions were deaerated by purging with dry nitrogen stream, and a slight nitrogen overpressure was kept during electrochemical experiments.

Preparation of Au-Cu-Pt/GCE electrodes

The scheme of preparation processes of the Au-Cu-Pt/GCE electrodes is shown in Scheme 1. Prior to modification, a bare glassy carbon electrode (GCE, 3mm in diameter, CH Instruments CO., Ltd., China) was polished with 0.3 μm alumina slurry to obtain a mirror surface, and then rinsed with doubly distilled water in an ultrasonic bath and dried for the use of following experiment. Firstly, the $HAuCl_4$/$CuSO_4$/0.5 M H_2SO_4 solutions with Au:Cu (by molar ratio) of 1:1, 1:5, 1:10 and 1:20 were prepared, respectively. Then Au-Cu nanoparticles were co-electrodeposited onto bare GCE in a $HAuCl_4$/$CuSO_4$/0.5 M H_2SO_4 solution at a constant potential of –0.4 V. After that, the Au-Cu nanoparticles modified GCE was immerged into a 2 mM H_2PtCl_6/0.5 M H_2SO_4 solution for 10 minutes. The Cu was partially replaced by Pt as the following reaction during the process:[27,28]

$$Cu/GCE + [PtCl_6]^{2-} \rightarrow Pt\text{-}Cu/GCE + Cu^{2+} + 6Cl^- \quad (1)$$

Then the as-prepared electrodes were rinsed with doubly distilled water to remove the residual ions. The as-obtained electrodes prepared in the $HAuCl_4$/$CuSO_4$/0.5 M H_2SO_4 solutions with Au:Cu of 1:1, 1:5, 1:10, and 1:20 were designated as Au-Cu-Pt/GCE-1, Au-Cu-Pt/GCE-5, Au-Cu-Pt/GCE-10 and Au-Cu-Pt/GCE-20, respectively.

Meanwhile, in order to determine the optimum charge of co-electrodepositing, a series of Au-Cu-Pt/GCE-10 electrodes were prepared with the charge of 2×10^{-3} C, 5×10^{-3} C, 1×10^{-2} C, 2×10^{-2} C, respectively. After Cu was partially replaced by Pt, the catalytic activity of as-prepared catalysts toward MEO was evaluated via cyclic voltammetry measurement. According to the experimental results, the electrode that was electrodeposited with the charge of 5×10^{-3} C had the highest peak current density, indicating that the charge of 5×10^{-3} C was optimum for the electrode preparation.

Additionally, another two electrodes, Pt/GCE and Au/GCE, were prepared for comparison. For Pt/GCE and Au/GCE, Pt and Au particles were directly electrodeposited onto bare GCE with the charge of 5×10^{-3} C, respectively. And the as-prepared electrodes were rinsed with doubly distilled water as well for the following use.

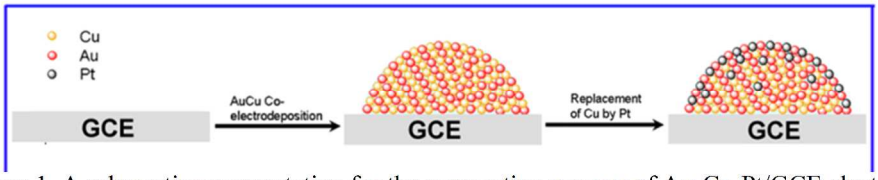

Scheme 1. A schematic representation for the preparation process of Au-Cu-Pt/GCE electrode.

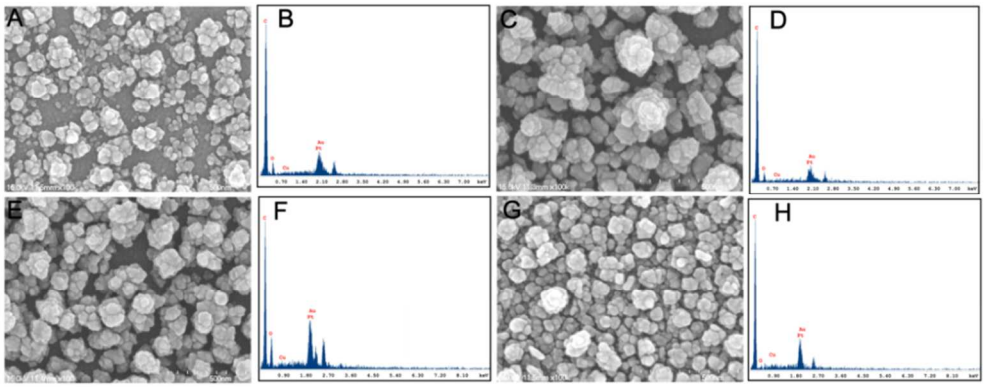

Fig. 1. SEM images of Au-Cu-Pt/GCE-1 (A), Au-Cu-Pt/GCE-5 (C), Au-Cu-Pt/GCE-10 (E), and Au-Cu-Pt/GCE-20 (G) electrodes and EDX spectra of Au-Cu-Pt/GCE-1 (B), Au-Cu-Pt/GCE-5 (D), Au-Cu-Pt/GCE-10 (F), and Au-Cu-Pt/GCE-20 (H) electrodes.

Table 1 Summarized the mole ratio of Au, Cu and Pt obtained by EDX analysis and the calculated amount of Au, Cu and Pt on different electrodes (μg on per GCE)

Electrodes	The mole ratio of Au, Cu and Pt			The calculated amount of Au, Cu and Pt (μg on per GCE)		
	Au	Cu	Pt	Au	Cu	Pt
Au-Cu-Pt/GCE-1	1	0.28	0.11	2.55	0.23	0.29
Au-Cu-Pt/GCE-5	1	0.90	0.55	1.45	0.42	0.79
Au-Cu-Pt/GCE-10	1	1.82	1.11	0.93	0.54	1.0
Au-Cu-Pt/GCE-20	1	2.42	1.80	0.68	0.53	1.21
Pt/GCE	-	-	1	-	-	2.53
Au/GCE	1	-	-	3.40	-	-

Characterization and electrochemical measurement

All the electrochemical experiments were performed on a CHI760E potentiostat/galvanostat (CH Instrumental Co., Ltd., China) with a conventional three-electrode-cell at room temperature. Platinum wire and saturated calomel electrode (SCE) were used as counter electrode and reference electrode, respectively. The modified glassy carbon electrode (GCE) was used as working electrode.

Scanning electron microscope (SEM, S–4700, Japan) and energy dispersive X-ray analysis (EDX, S-4700, Japan) were performed to obtain the morphology and the composition of the as-prepared catalysts. EDX element mapping was applied to observe the distribution of elements on the surface of the sample. X-ray photoelectron spectroscopy (XPS) was obtained on an ESCALab220i-XL electron spectrometer from VG Scientific with 300 W Al Kα X-ray radiation as the X-ray source for excitation.

Results and discussion

Characterizations of as-prepared electrodes

The surface morphology of the prepared Au-Cu-Pt/GCE-1 (A), Au-Cu-Pt/GCE-5 (C), Au-Cu-Pt/GCE-10 (E) and Au-Cu-Pt/GCE-20 (G) electrodes were characterized by scanning electron microscopy (SEM). As Fig. 1 displayed, different electrodes show different morphologies. As seen clearly in Fig. 1A, most of the catalyst particles on Au-Cu-Pt/GCE-1 are scattered sparsely on GCE and few particles are piled up into little cluster. While on Au-Cu-Pt/GCE-5 (Fig. 1C), the particles grow into clusters like flowers. For Au-Cu-Pt/GCE-10 in Fig. 1E, although the morphology of the catalyst particles is similar to that on Au-Cu-Pt/GCE-5 (Fig. 1C), the flower-like clusters are distributed relatively homogeneously and uniformly on Au-Cu-Pt/GCE-10. And the SEM image of Au-Cu-Pt/GCE-20 is shown in Fig. 1G, the catalyst particles spread densely (shown in Fig. 1G), which might lead to the decrease of surface area of catalyst in comparison with Au-Cu-Pt/GCE-10.

The composition of the Au-Cu-Pt/GCE electrodes was analyzed by EDX analysis in Fig. 1B, D, F and H, respectively. The results confirm the presence of Au, Cu and Pt elements. The existence of Au, Cu and Pt also proved that Au-Cu-Pt nanoparticles were successfully loaded on the surface of GCE. Meanwhile, Table 1 summarizes the molar ratio of Au, Cu and Pt obtained by EDX analysis on each GCE and the calculated amounts of Au, Cu and/or Pt according to the Faraday's Law ($Q = nz$F). As seen from Table 1, the amount of Pt loading on Au-Cu-Pt/GCE-20 (1.21 μg) is the largest among the Au-Cu-Pt/GCE electrodes, and it is still half of that amount on Pt/GCE (2.53 μg). The results prove that the simple two-step method may be a usful method to reduce the amount of platinum catalyst used in the DMFC.

EDX element mapping was further applied to observe the distribution of elements on the surface of Au-Cu-Pt/GCE-10 electrode, as shown in Fig. 2. Fig. 2B, C and D reveal that the Au, Cu and Pt elements are similarly distributed on the surface of the electrode. The similar element distribution of these elements indicates that there may be some contact among the Au, Cu and Pt particles and/or elements. Additionally, it seems that the distribution of Cu on the surface of electrode is less dense than that of Pt, which successfully demonstrated that Cu was partially replaced by Pt on the surface of electrode.

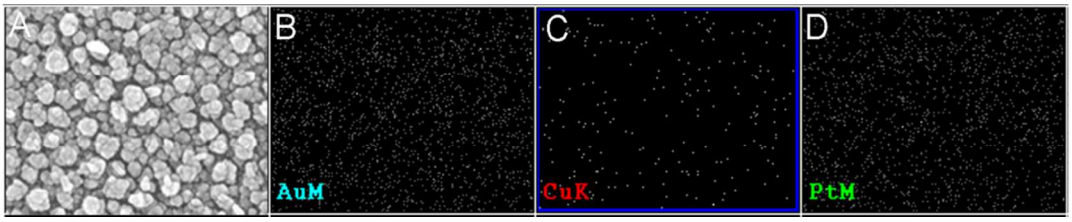

Fig. 2 EDX element mapping of Au-Cu-Pt/GCE-10 electrode (A) and its Au (B), Cu (C) and Pt (D) element distribution.

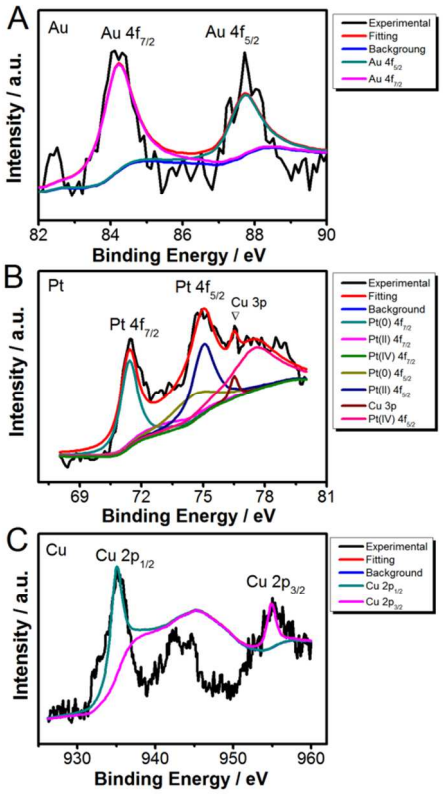

Fig. 3. XPS spectra of (A) Au 4f region; (B) Pt 4f region; and (C) Cu 2p region of Au-Cu-Pt/GCE-10. The spectra were obtained by calibration based on C 1s peak at 284.5 eV.

X-ray photoelectron spectroscopy (XPS) measurements are generally used to further measure the composition of the nanoparticles and to verify the valance states of the nanoparticles. Fig. 3A shows the Au 4f spectrum of Au-Cu-Pt-10 ternary catalyst. The signal of Au 4f component could be resolved into two typical well-separated doublets at about 84.2 and 87.7 eV binding energy (BE), assigned to the binding energy of Au $4f_{7/2}$ and Au $4f_{5/2}$ in zero-valent state,[29,30] respectively. It is apparent that the Au0 peaks are shifted toward a higher BE in comparison with bulk Au, which is probably due to the alloying with Cu and Pt during the fabrication process.[31,32] The Pt 4f spectrum of Au-Cu-Pt-10 composite catalyst is shown in Fig. 3B. The Pt 4f signal could be resolved into six doublets. Two intense peaks of Pt 4f component at 71.4 and 74.5 eV (BE) are assigned to Pt $4f_{7/2}$ and Pt $4f_{5/2}$ of metallic Pt, respectively. Two peaks observed at 72.3 and 75.0 eV can be assigned to Pt $4f_{7/2}$ and Pt $4f_{5/2}$ components of Pt (II) in PtO and $Pt(OH)_2$-like species.[6,33] These two doublets show a slightly negative shift, which is probably due to the geometry effect (lattice constrain) and electronic effect (binding energy modification) between Pt, Au and/or Cu atomic orbit and in turn to their alloy formation.[34,35] Meanwhile, two additional Pt 4f peaks at BE ca. 74.2 and 77.5 eV are corresponding to a higher oxidation state Pt (Ⅳ).[36] In addition, it should be noteworthy that there is an obvious peak at 76.5 eV, which is assigned to the Cu 3p.[19,28] In the case of copper (Fig. 3C), the Cu 2p signal was deconvoluted into two distinguishable doublets at 935.0 and 954.9 eV, which is corresponding to Cu $2p_{3/2}$ and Cu $2p_{1/2}$ of metallic Cu, respectively. Similarly, the BE signals of Cu 2p were shifted compared with the reports in literature,[19,37] which is owing to the alloying with Au and Pt. Besides, the broad peak at ca. 940 eV can be observed, pointing to the presence of oxidized Cu (II) species.[28] According to the above results, it can be found that Au and most of Pt and Cu are existed in metallic state; and the alloying micro-structures exist in the catalyst among Au, Cu and/or the partially replaced Pt during the fabrication process.

The catalytic performances of as-prepared electrodes

Fig. 4A presents the cyclic voltammograms (CVs) in 0.5 M H_2SO_4 aqueous solution on Au-Cu-Pt/GCE-1 (a), Au-Cu-Pt/GCE-5 (b), Au-Cu-Pt/GCE-10 (c) and Au-Cu-Pt/GCE-20 (d), Pt/GCE (e), and Au/GCE (f), respectively. And Fig. 4B is the partial magnification of CVs. It can be seen that the CVs of these electrodes exhibit similar profiles to each other. The broad peak at the potential region from 0.1 to 0.5 V on each electrode is assigned to the redox of the Au, Cu and/or Pt oxides in catalysts. Meanwhile, hydrogen adsorption/desorption peaks are observed obviously in the range between −0.25 and 0 V during the scan.[38] The electrochemical active surface area (ECSA) of the composite electrodes can be derived by the integrated charge of hydrogen adsorption/desorption peak in CVs (inset in Fig.4A) according to eq. (2):[39-41]

$$ECSA_{Pt} = Q_H/0.21\times[Pt] \quad (2)$$

where Q_H in mC is the integrated charge of the hydrogen adsorption/desorption peaks in CVs; [Pt] represents the platinum loading (mg) in the electrode, and the constant 0.21 in mC cm^{-2} is assumed as the maximum surface charge transferred to Pt during adsorption of a real monolayer of H. By calculated, the $ECSA_{Pt}$ of the electrodes was estimated to be 8.5 $m^2 g^{-1}$ (Au-Cu-Pt/GCE-1), 24.4 $m^2 g^{-1}$ (Au-Cu-Pt/GCE-5), 32.9 $m^2 g^{-1}$ (Au-Cu-Pt/GCE-10), 23.2 $m^2 g^{-1}$ (Au-Cu-Pt/GCE-20), 30.6 $m^2 g^{-1}$ (Pt/GCE). Au-Cu-Pt/GCE-10 presented the largest $ECSA_{Pt}$ (32.9 $m^2 g^{-1}$) compared with the other Au-Cu-Pt/GCE electrodes. This is probably ascribed to the more Pt loadings and the relatively homogenous distribution of nanoparticles on Au-Cu-Pt/GCE-10.[41] As compared with Pt/GCE, the amount of Pt loading on Au-Cu-Pt/GCE-10 is less than that on Pt/GCE (Table 1), nevertheless, the $ECSA_{Pt}$ on Au-Cu-Pt/GCE-10 is larger than that on Pt/GCE. The largest $ECSA_{Pt}$ indicates the Au-Cu-Pt/GCE-10 has the greatest catalytic activity.

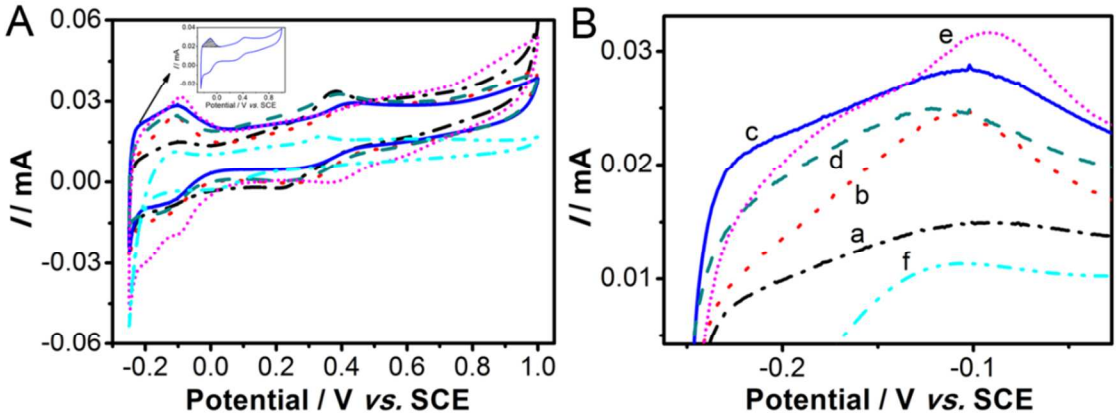

Fig. 4. (A) Cyclic voltammograms (CVs) of Au-Cu-Pt/GCE-1 (a), Au-Cu-Pt/GCE-5 (b), Au-Cu-Pt/GCE-10 (c), Au-Cu-Pt/GCE-20 (d), Pt/GCE (e), and Au/GCE (f) in 0.5 M H_2SO_4 solution at a scan rate of 50 mV s^{-1}. (B) The partial magnification of CVs in Fig. 3A.

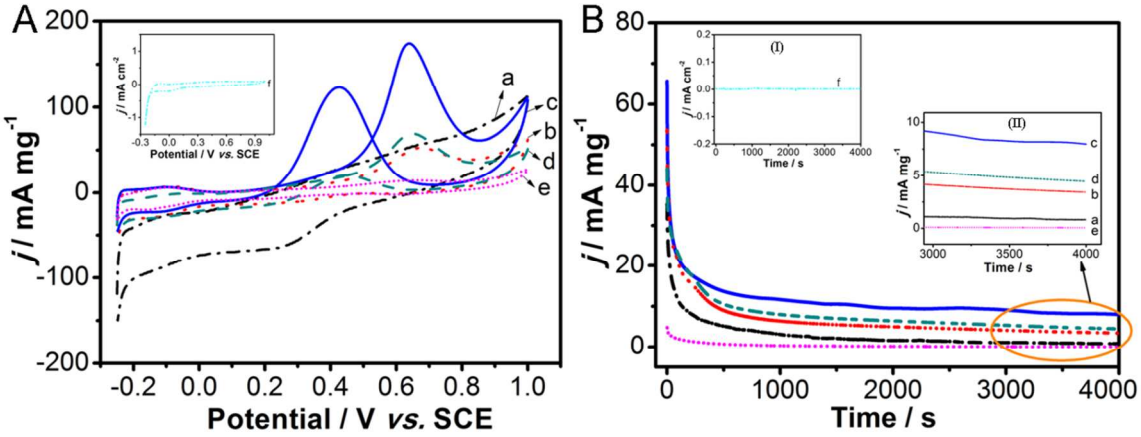

Fig. 5. (A) Cyclic voltammograms (CVs) and (B) Chronoamperograms (CAs) of Au-Cu-Pt/GCE-1 (a), Au-Cu-Pt/GCE-5 (b), Au-Cu-Pt/GCE-10 (c), Au-Cu-Pt/GCE-20 (d), Pt/GCE (e), and Au/GCE (f) at 0.55 V in 1.0 M CH_3OH/0.5 M H_2SO_4 solution, respectively. Scan rate: 50 mV s^{-1}.

The catalytic activity of the as-prepared electrodes toward MEO was measured by cyclic voltammetry. Fig. 5A presents the CVs of Au-Cu-Pt/GCE-1 (a), Au-Cu-Pt/GCE-5 (b), Au-Cu-Pt/GCE-10 (c) and Au-Cu-Pt/GCE-20 (d), Pt/GCE (e), and Au/GCE (f) electrodes in an aqueous solution containing 1.0 M CH_3OH and 0.5 M H_2SO_4. For Au/GCE, the current density was normalized by the surface area of GCE (0.07 cm^{-2}) due to no existence of Pt, shown in the inset in Fig. 5A. There is no obvious oxidation peak observed on Au/GCE electrode, which is probably owing to no effective catalytic component like Pt in Au/GCE. And the current densities on the other electrodes in all the following electrochemical tests were normalized by the mass of Pt loading on per GCE. As seen, the oxidation peak between 0.4 and 0.9 V in the forward scan is related to the direct oxidation of methanol species, which were strongly adsorbed onto the catalyst surface. And there is a peak observed between 0.2 and 0.7 V during the reverse scan, which is related to the oxidation of methanol byproducts or its residues during the forward scan.[36,41] While on Au-Cu-Pt/GCE-1, the oxidation peak toward MEO in the forward scan was difficult to distinguish, which may be due to the low Pt loading and/or the extremely small $ECSA_{Pt}$ on Au-Cu-Pt/GCE-1. The observed peak current densities in the forward scan on the other electrodes are 51.39 mA mg^{-1} (Au-Cu-Pt/GCE-5), 174.31 mA mg^{-1} (Au-Cu-Pt/GCE-10), 69.42 mA mg^{-1} (Au-Cu-Pt/GCE-20), 14.39 mA mg^{-1} (Pt/GCE), respectively. The Au-Cu-Pt/GCE-10 electrode presented the largest peak current density, suggesting that it possessed the highest catalytic activity for MEO. It also suggests the simple two-step method can effectively decrease the Pt usage in catalyst. And the current densities on Au-Cu-Pt/GCE-5, Au-Cu-Pt/GCE-10 and Au-Cu-Pt/GCE-20 are much higher than that on Pt/GCE. Especially for the Au-Cu-Pt/GCE-10 with rather low amount of Pt loadings, it has a superior mass current density of 174.31 mA mg^{-1}, which is over 12 times as high as that on Pt/GCE. This is probably ascribed to the electronic effect and synergetic effect among Au, Cu and/or Pt in the Au-Cu-Pt ternary catalyst. The co-electrodeposition and the replacement reaction among Au, Cu and/or Pt to some extent change the surface electron structure of Pt catalyst, which weakens the adsorption of intermediate species on Pt during MEO.[42,43] And the synergetic effect between the second/third co-catalyst (Au, Cu) and Pt would increase the poisoning tolerance of catalyst toward COads, consequently promoting the catalytic activity.[10,44,45]

Chronoamperometry was used to examine the catalytic stability of the electrodes. Fig. 5B records the chronoamperograms (CAs) of Au-Cu-Pt/GCE-1 (a), Au-Cu-Pt/GCE-5 (b), Au-Cu-Pt/GCE-10 (c) and Au-Cu-Pt/GCE-20 (d),

Pt/GCE (e), and Au/GCE (f) at a constant potential of 0.55 V in 1.0 M CH_3OH/0.5 M H_2SO_4, respectively. Similarly to the CVs in Fig. 5A, the CAs on Au/GCE was normalized by the surface area of GCE as well, recorded in the inset (I) in Fig. 5B. It can be seen that the current density on Au/GCE during the whole scan was kept at a very weak situation. For the other electrodes, the initial current density was in a sequence of Au-Cu-Pt/GCE-10 (65.7 mA mg^{-1}) > Au-Cu-Pt/GCE-5 (53.6 mA mg^{-1}) > Au-Cu-Pt/GCE-20 (44.1 mA mg^{-1}) > Au-Cu-Pt/GCE-1 (35.3 mA mg^{-1}) > Pt/GCE (4.8 mA mg^{-1}). Subsequently, the current densities on all electrodes undergo an inevitable decrease at the initial stage, which were probably due to the unavoidable formation of Pt-oxides and poisoning intermediates generated during MEO.[46,47] After scanning for 4000 s, the value of current density on each electrode is in a sequence of Au-Cu-Pt/GCE-10 (c) > Au-Cu-Pt/GCE-20 (d) > Au-Cu-Pt/GCE-5 (b) > Au-Cu-Pt/GCE-1 (a) > Pt/GCE (e), as shown as the partial magnification in the inset (II). All Au-Cu-Pt/GCE electrodes still present much higher current densities than Pt/GCE. This is probably attributed to the synergetic effect among Au, Cu and Pt in the ternary catalyst, which enhances the poisoning tolerance of catalyst toward COads. What is more, Au-Cu-Pt/GCE-10 presents the largest current density, indicating that the Au-Cu-Pt/GCE-10 electrode has the highest stability for MEO compared to other electrodes.

Electrochemical impedance spectroscopy study

In order to evaluate the electrochemical properties of a series of as-prepared Au-Cu-Pt/GCE electrodes, electrochemical impedance spectroscopy (EIS) were carried out on the Au-Cu-Pt/GCE-1 (a), Au-Cu-Pt/GCE-5 (b), Au-Cu-Pt/GCE-10 (c) and Au-Cu-Pt/GCE-20 (d) at electrode potential of 0.4 V in 1.0 M CH_3OH/0.5 M H_2SO_4 solution, respectively. The Nyquist plots were recorded in Fig. 6. It can be seen that the diameters of impedance arc (DIAs) on the electrodes decreases in the following order: Au-Cu-Pt/GCE-1 > Au-Cu-Pt/GCE-5 > Au-Cu-Pt/GCE-20 > Au-Cu-Pt/GCE-10. The DIA on Au-Cu-Pt/GCE-10 is the smallest in comparison with those on other electrodes, demonstrating that Au-Cu-Pt/GCE-10 has the lowest charge transfer resistance compared with other electrodes.[40,48,49] It is probably due to the well-proportional distribution of metal atoms and the relatively homogeneous distribution of Au-Cu-Pt nanoparticles on Au-Cu-Pt/GCE-10.

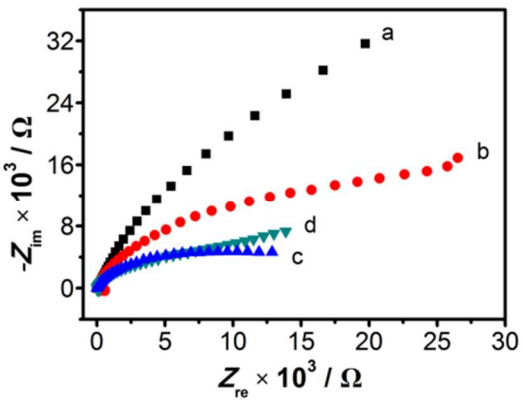

Fig. 6. EIS Nyquist plots of methanol electrooxidation on Au-Cu-Pt/GCE-1 (a), Au-Cu-Pt/GCE-5 (b), Au-Cu-Pt/GCE-10 (c) and Au-Cu-Pt/GCE-20 (d) electrodes in 1.0 M CH_3OH/0.5 M H_2SO_4 solution at electrode potentials of 0.4 V.

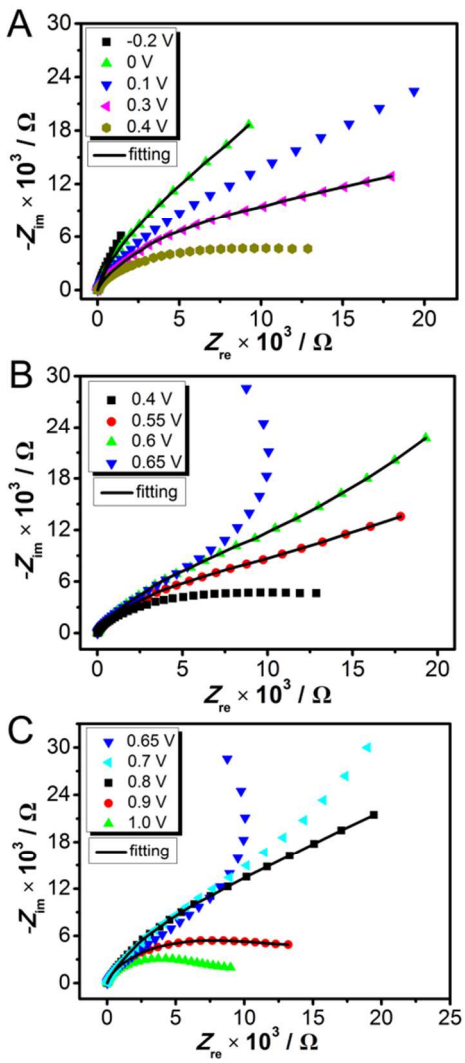

Fig. 7. Nyquist plots of methanol electrooxidation on Au-Cu-Pt/GCE-10 electrode in 1.0 M CH_3OH/0.5 M H_2SO_4 solution at electrode potentials from –0.2 to 1.0 V. The fitting lines in (A–C) are representative simulations based on the equivalent circuits in Fig. 7A and B, respectively.

The interfacial processes as well as the electron transfer kinetics of MEO on Au-Cu-Pt/GCE-10 were further studied by EIS at selected potentials in the range of –0.2 to 1.0 V. Figs. 7A-C show the Nyquist plots of methanol oxidation on Au-Cu-Pt/GCE-10 in 0.5 M H_2SO_4 solution containing 1.0 M CH_3OH at different electrode potentials, respectively. Generally, the MEO shows different impedance behaviors at different electrode potentials.[49,50] For example, as Fig. 7A displayed, there is a decrease in DIAs on Au-Cu-Pt/GCE-10 with the increase of the applied potential from –0.2 to 0.4 V. As the potential increases in the range of 0.4 to 0.6 V (Fig. 7B), the DIAs begin to increase. This can be explained that since the onset potential of methanol oxidation on Au-Cu-Pt/GCE-10 is at about 0.2 V (CVs in Fig. 5A). The initially decreased DIAs between –0.2 and 0.4 V indicate that more and more active sites are available for MEO, owing to the oxidation removal of CO-like intermediate species occurred at low potentials. Also it suggests the rate of MEO on Au-Cu-Pt/GCE-10 is accelerated. As the methanol oxidation reaction continued, some poisoning intermediates (e.g. COads) accumulated gradually on the

surface of Au-Cu-Pt/GCE-10, resulting in the increase in the DIA at higher potentials. At the applied potential of 0.65 V, the arc takes a reverse change obviously. It is probably attributed to the gradual recovery of the catalytic active sites because of the oxidation removal of COads. However, the arc remains in the first quadrant instead of further reversing to the second quadrant as some other research reported.[40,51] And with the potential continues to increasing, (Fig. 7C), the arcs resume to the conventional profile with large DIA and the DIA keeps decreasing. This is due to that CO-like intermediate species were removed timely at high potential.

The equivalent circuit is used to fit the EIS data.[40,49] On the basis of the above impedance measurements in Fig. 7(A-C), two equivalent circuits for Au-Cu-Pt/GCE-10 are proposed in Fig. 8. The element R_s represents the solution resistance from the relative electrode and the working electrode, R_{ct} is the charge-transfer resistance, and CPE_1 (constant phase element) is the electrode double layer capacitance instead of a capacitor, which is used to account for some complex element on the porous catalysts in the whole system. CPE_2 and resistor (R_e) in Fig. 8A are added in series to fit the high frequency impedance data, which are attributed to a charge-transfer process at the outermost surface of the electrode. And R_o and O_{rea} in Fig. 8B denote the risistance and relaxation capacitive behavior of electrode for MEO, respectively. Some representative fittings for the Au-Cu-Pt/GCE-10 electrode are shown as solid lines in Fig. 7 (A-C), which shows good agreement with the corresponding experimental data.

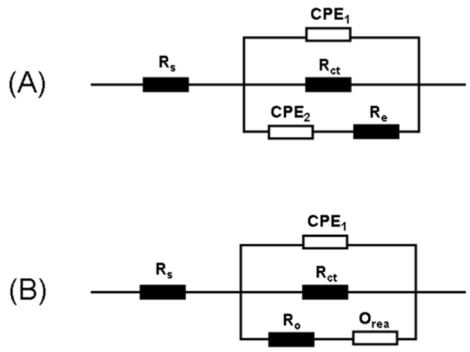

Fig. 8. Equivalent circuits used for simulating the impedance spectra for methanol electrooxidation on Au-Cu-Pt/GCE-10 electrode at different potentials: (A) at –0.2 to 0.4 V, and 0.7 to 1.0 V, (B) at 0.55 to 0.65 V.

Conclusions

Using the simple two-step method, Au-Cu-Pt/GCE electrodes were fabricated successfully with some alloying micro-structure. Although the amount of Pt loading were reduced significantly, the catalytic activity was enhanced compared with Pt/GCE. The enhanced activity may be described to the relatively homogenous distribution of Au-Cu-Pt nanoparticles and the electronic effect as well as synergetic effect among Au, Cu and/or Pt. Besides, the EIS behavior of MEO on the Au-Cu-Pt/GCE electrodes were also studied, which showed that the charge-transfer resistance for MEO on Au-Cu-Pt/GCE-10 is the smallest compared to that on Au-Cu-Pt/GCE-20, Au-Cu-Pt/GCE-5 and Au-Cu-Pt/GCE-1. On the basis of the above results, it is anticipated that Au-Cu-Pt/GCE-10 will show great potential as an excellent electrocatalyst for methanol fuel cell applications.

Acknowledgements

This work was supported by the National Natural Science Foundation of China (Grant Nos. 51373111, 51073114, 20933007), the Project of Scientific and Technologic Infrastructure of Suzhou (SZS201207), Suzhou Nano-project (ZXG2012022), the Priority Academic Program Development of Jiangsu Higher Education Institutions (PAPD), and the Academic Award for Young Graduate Scholar of Soochow University, the Opening Project of Xinjiang Key Laboratory of Electronic Information Materials and Devices (XJYS0901–2010–01).

Notes and references

College of Chemistry, Chemical Engineering and Materials Science, Soochow University, Suzhou 215123, PR China. Tel: 86-512-65880089, Fax: 86-512-65880089; E-mail: duyk@suda.edu.cn (Y. Du)

1 J. Chang, L. Feng, C. Liu, W. Xing and X. Hu, *Energy & Environmental Science*, 2014, **7**, 1628.
2 L. Guo, S. Chen, L. Li and Z. Wei, *Journal of Power Sources*, 2014, **247**, 360.
3 Y. Cheng and S. P. Jiang, *Electrochimica Acta*, 2013, **99**, 124.
4 E. Antolini and E. R. Gonzalez, *Catalysis Today*, 2011, **160**, 28.
5 Y.S. Wang, S.Y. Yang, S.M. Li, H.W. Tien, S.T. Hsiao, W.H. Liao, C.H. Liu, K.H. Chang, C.C. M. Ma and C.C. Hu, *Electrochimica Acta*, 2013, **87**, 261.
6 F.F. Ren, C.Q. Wang, C.Y. Zhai, F.X. Jiang, R.R. Yue, Y.K. Du, P. Yang and J.K. Xu, *Journal of Materials Chemistry A*, 2013, **1**, 7255.
7 T. G. Kelly and J. G. Chen, *Chemical Society Reviews*, 2012, **41**, 8021.
8 C.J. Zhong, J. Luo, P.N. Njoki, D. Mott, B. Wanjala, R. Loukrakpam, S. Lim, L. Wang, B. Fang and Z. Xu, *Energy & Environmental Science*, 2008, **1**, 454.
9 F. Cheng and J. Chen, *Chemical Society Reviews*, 2012, **41**, 2172.
10 Y. Xu and B. Zhang, *Chemical Society Reviews*, 2014, **43**, 2439.
11 Z. Zhang, J. Liu, J. Gu, L. Su and L. Cheng, *Energy & Environmental Science*, 2014, **7**, 2535.
12 C. Della Pina, E. Falletta and M. Rossi, *Chemical Society Reviews*, 2012, **41**, 350.
13 Z. Guo, B. Liu, Q. Zhang, W. Deng, Y. Wang and Y. Yang, *Chemical Society Reviews*, 2014, **43**, 3480.
14 W. Zhong, Y. Liu and D. Zhang, *Journal of Physical Chemistry C*, 2012, **116**, 2994.
15 M. Yin, Y. Huang, L. Liang, J. Liao, C. Liu and W. Xing, *Chemical communications*, 2011, **47**, 8172.
16 M.-Y. Duan, R. Liang, N. Tian, Y.-J. Li and E. S. Yeung, *Electrochimica Acta*, 2013, **87**, 432.
17 J. Suntivich, Z. Xu, C. E. Carlton, J. Kim, B. Han, S. W. Lee, N. Bonnet, N. Marzari, L. F. Allard, H. A. Gasteiger, K. Hamad-Schifferli and Y. Shao-Horn, *Journal of the American Chemical Society*, 2013, **135**, 7985.
18 H. Yang, L. Dai, D. Xu, J. Fang and S. Zou, *Electrochimica Acta*, 2010, **55**, 8000.
19 M. Ammam and E. B. Easton, *Journal of Power Sources*, 2013, **222**, 79.
20 Y.-X. Wang, H.-J. Zhou, P.-C. Sun and T.-H. Chen, *Journal of Power Sources*, 2014, **245**, 663.

21 Y. Zhang, Y.-e. Gu, S. Lin, J. Wei, Z. Wang, C. Wang, Y. Du and W. Ye, *Electrochimica Acta*, 2011, **56**, 8746.
22 N. Tsiouvaras, M. V. Martínez-Huerta, O. Paschos, U. Stimming, J. L. G. Fierro and M. A. Peña, *International Journal of Hydrogen Energy*, 2010, **35**, 11478.
23 Y. Huang, Y. Guo, Y. Wang and J. Yao, *International Journal of Hydrogen Energy*, 2014, **39**, 4274.
24 M. Ammam, L. E. Prest, A. D. Pauric and E. B. Easton, *Journal of the Electrochemical Society*
J. Electrochem. Soc., 2012, **159**, B195.
25 M. Ammam and E. B. Easton, *Journal of the Electrochemical Society*, 2012, **195**, B635.
26 W. Hong, J. Wang and E. Wang, *Small*, 2014.
27 B. Geboes, I. Mintsouli, B. Wouters, J. Georgieva, A. Kakaroglou, S. Sotiropoulos, E. Valova, S. Armyanov, A. Hubin and T. Breugelmans, *Applied Catalysis B: Environmental*, 2014, **150-151**, 249.
28 I. Mintsouli, J. Georgieva, S. Armyanov, E. Valova, G. Avdeev, A. Hubin, O. Steenhaut, J. Dille, D. Tsiplakides, S. Balomenou and S. Sotiropoulos, *Applied Catalysis B: Environmental*, 2013, **136-137**, 160.
29 R.K. Shervedani and A.Amini, *Electrochimica Acta*, 2014, **121**, 376.
30 D. P. Anderson, R. H. Adnan, J. F. Alvino, O. Shipper, B. Donoeva, J.-Y. Ruzicka, H. Al Qahtani, H. H. Harris, B. Cowie, J. B. Aitken, V. B. Golovko, G. F. Metha and G. G. Andersson, *Physical Chemistry Chemical Physics*, 2013, **15**, 14806.
31 P. Wang, Z.G. Liu, X. Chen, F.L. Meng, J.H. Liu and X.J. Huang, *Journal of Materials Chemistry A*, 2013, **1**, 9189.
32 K. Qian, L. Luo, H. Bao, Q. Hua, Z. Jiang and W. Huang, *Catalysis Science & Technology*, 2013, **3**, 679.
33 N. Ilayaraja, N. Prabu, N. Lakshminarasimhan, P. Murugan and D. Jeyakumar, *Journal of Materials Chemistry A*, 2013, **1**, 4048.
34 Z. Xu, H. Zhang, S. Liu, B. Zhang, H. Zhong and D.S. Su, *International Journal of Hydrogen Energy*, 2012, **37**, 17978.
35 J. B. Xu, T. S. Zhao, W. W. Yang and S. Y. Shen, *International Journal of Hydrogen Energy*, 2010, **35**, 8699.
36 S. Sharma, A. Ganguly, P. Papakonstantinou, X. Miao, M. Li, J. L. Hutchison, M. Delichatsios and S. Ukleja, *Journal of Physical Chemistry C*, 2010, **114**, 19459.
37 A. Gutie´rrez, C. Alonso, M. F. Lo´pez and M. L. Escudero, *Surface Science* 1999, **430**, 206.
38 H. Zhang, F. Jiang, R. Zhou, Y. Du, P. Yang, C. Wang and J. Xu, *International Journal of Hydrogen Energy*, 2011, **36**, 15052.
39 U. M, K. M, M. M and U. I, *Electrochim Acta*, 2003, **48**, 1367.
40 W.Q. Zhou, Y.K. Du, F.F. Ren, C.Y. Wang, J.K. Xu and P. Yang, *International Journal of Hydrogen Energy*, 2010, **35**, 3270.
41 Y. J. Li, W. Gao, L. J. Ci, C. M. Wang and P. M. Ajayan, *Carbon*, 2010, **48**, 1124.
42 J. Luo, P. N. Njoki, Y. Lin, D. Mott, L. Wang and C.J. Zhong, *Langmuir*, 2006, **22**, 2892.
43 D. Mott, J. Luo, P. N. Njoki, Y. Lin, L. Wang and C.J. Zhong, *Catalysis Today*, 2007, **122**, 378.
44 P. Liu, X. Ge, R. Wang, H. Ma and Y. Ding, *Langmuir*, 2009, **25**, 561.
45 X.Ge, R. Wang, P. Liu and Y. Ding, *Chem. Mater.*, 2007, **19**, 5827.
46 Y.M. Li, L.H. Tang and J.H. Li, *Electrochemistry Communications*, 2009, **11**, 846.
47 C.Q. Wang, F.X. Jiang, R.R. Yue, H.W. Wang and Y.K. Du, *Journal of Solid State Electrochemistry*, 2014, **18**, 515.
48 Z.B. Wang, G.P. Yin, Y.Y. Shao, B.Q. Yang, P.F. Shi and P.X. Feng, *Journal of Power Sources*, 2007, **165**, 9.
49 R.R. Yue, Q. Zhang, C.Q. Wang, Y.K. Du, P. Yang and J.K. Xu, *Electrochimica Acta*, 2013, **107**, 292.
50 W. Sugimoto, K. Aoyama, T. Kawaguchi, Y. Murakami and Y. Takasu, *Journal of Electroanalytical Chemistry*, 2005, **576**, 215.
51 H.P. Yuan, D.J. Guo, X.P. Qiu, W.T. Zhu and L.Q. Chen, *Journal of Power Sources*, 2009, **188**, 8.

